JOURNAL OF GEOPHYSICAL RESEARCH, VOL. 105, NO. D4, PAGES 4587–4606, FEBRUARY 27, 2000

Analysis of ocean surface heat fluxes in a NOGAPS climate simulation: Influences from convection, clouds and dynamical processes

Duane E. Waliser

Institute for Terrestrial and Planetary Atmospheres, State University of New York, Stony Brook

Timothy F. Hogan

Naval Research Laboratory, Monterey, California

Abstract. This study examines the simulation quality of the surface heat flux fields produced during a climate simulation of the Navy Operational Global Atmospheric Prediction System, version 3.4, with a reduced spectral truncation of T63 and 18 levels (herineafter referred to as NOGAPS-CL). Comparisons are made between a 17-year NOGAPS-CL simulation using monthly sea surface temperatures as surface boundary conditions and a number of validating data sets consisting of ship, satellite, and/or reanalysis-based surface heat fluxes, precipitation, top of the atmosphere radiation budget, water vapor, cloud frequency, surface wind stress, and tropospheric winds. In this extended, long-range integration, NOGAPS-CL underpredicts the net surface shortwave flux in much of the subtropical oceans and overpredicts the net shortwave flux in the western Pacific warm pool and the midlatitude oceans, when compared to several satellite-derived climatological data sets. In addition, NOGAPS-CL over predicts the latent heat flux in much of the subtropics and under predicts the latent heat flux over the northern ocean western boundary currents and under the storm track regions that extend eastward from them. These shortwave and evaporation biases combine to produce errors in the surface net heat flux, with too little heat entering the subtropical/tropical oceans and too much heat loss in the midlatitudes oceans. Examination of related quantities indicates that the tropical climate biases are coupled to shortcomings in the convective cloud and/or boundary layer parameterizations which leads to the premature release of moist instability from the boundary layer in regions just outside the deep convective zones. This leads to enhanced climatological cloudiness, rainfall, and surface evaporation, as well as to a reduction in the surface shortwave flux and outgoing longwave radiation (OLR), in the subtropical regions. Furthermore, because of this early release of the moist static energy, there is a reduction in clouds, rainfall and water vapor content, as well as enhanced surface shortwave flux and outgoing longwave radiation, in the deep convective zones. The reduction in rainfall and enhanced OLR reduces the strength of the tropical large-scale circulation, which in turn reduces the strength of the subsidence in the subtropical regions which normally acts to suppress the convection processes in these regions. The implications of these results are discussed in terms of the relationship among the forecast model climatological surface fluxes, convection, clouds, and the dynamical processes, as well as their similarities to other climate models and their possible impact on the simulation of transient systems.

1. Introduction

The United States Navy Fleet Numerical Meteorology and Oceanography Center (FNMOC) is the Department of Defense (DoD) main source for standard meteorological and oceanographic (METOC) prediction products [*Nelson and Aldinger,* 1992]. At the heart of these predictions is the Navy Operational Global Atmospheric Prediction System (NOGAPS), a short- to medium-range (6 days) numerical weather forecast model that was developed and transitioned to FNMOC by the Marine Meteorology Division of the Naval Research Laboratory. The current operational system is version 4.0. This analysis and forecast system is a high-resolution global, spectral (triangular truncation of 159 waves with 24 vertical levels, T159l24), numerical weather prediction system utilizing real-time data, quality-controlled data assimilation, nonlinear normal mode initialization, along with sophisticated parameterizations of convection, cloud, radiation and boundary layer processes. The predictions provided by NOGAPS are vital in providing guidance for worldwide DoD operations and providing boundary conditions to other METOC ocean prediction systems [*Nelson and Aldinger,* 1992]. In the case of NOGAPS, *Hogan and Rosmond* [1991] and *Hogan and Brody* [1993] provide evidence for its useful and improving skill and emphasize the Navy's commitment to improving the NOGAPS skill in producing short- to medium-range numerical weather forecasts.

Paper number 1999JD901028.
0148-0227/00/1999JD901028$09.00

Research has also been conducted with lower-resolution versions (T47L18 and T63L18) of the NOGAPS 3.4 forecast model in a climate mode. The systematic errors evident in these low-resolution climate runs are not necessarily directly applicable to the high-resolution data assimilation runs but instead offer guidance on the long-term trends of the lower-resolution forecast model after the influence of the initial conditions become negligible. A 10-year T47L18 NOGAPS simulation was performed as part of the Atmospheric Model Intercomparison Project (AMIP) experiment [*Gates,* 1999]. The results of the climate simulation errors on the simulated Northern Hemisphere intraseasonal circulation anomalies were reported on by *Reynolds et al.* [1996] and the effects of climate model error on the propagation of extratropical waves were presented by *Reynolds and Gelaro* [1997]. An intercomparison of the hydrological processes of several climate model AMIP simulations (including NOGAPS 3.4) is given by *Lau et al.* [1996]. *Li and Hogan* [1999] conducted extended coupled climate simulations using MOM 2.0 coupled to the T47L18 NOGAPS 3.4. As with many other coupled climate systems, it was found that a flux correction was needed to adjust the tropical sea surface temperature field to obtain realistic seasonal and interannual variations. *Ridout and Reynolds* [1998] used a similar low-resolution version of NOGAPS in seasonal simulations to study the impact of convective triggering by boundary layer thermals in the western Pacific warm pool. They found that by constraining deep convection to conditions consistent with thermals, the excessive precipitation north of the warm pool was reduced. This allowed for an increased flux of moisture into the warm pool region and improved the precipitation, the precipitable water, and low-level winds in that region.

The focus of this study is to examine the simulation quality of the surface heat fluxes in a climate simulation of the NOGAPS 3.4 forecast model at a T63L18 resolution, with primary attention given to the net surface shortwave and latent heat fluxes. Of the four surface heat flux components (i.e., shortwave, longwave, latent, and sensible), the shortwave and latent fluxes play unique and prominent roles. In the case of the shortwave, over most of the year and for most of the ocean, it is the only surface flux representing heat input into the ocean. In the case of the latent heat flux, it not only represents the largest (globally averaged) heat loss term [e.g., *Wielicki et al.,* 1995] but it is also strongly coupled to the hydrological cycle. Climate model validation is performed on long-term averages using a variety of multiyear in situ, satellite-derived and reanalysis climatology data sets. In order to ascertain the underlying reasons for systematic errors in the model long-term climate surface flux fields, comparisons are performed on rainfall, cloud, column water vapor, 200 mbar velocity potential, surface wind stress, and top of the atmosphere radiation data. In the next section the model and the simulation framework are described. In Section 3, the validating data sets are described. In section 4 the results of the model-data comparisons and associated analysis are presented. Section 5 concludes with a summary of the results and a discussion of their implications.

2. Model Experiments

A description of the dynamics and physics of NOGAPS 3.4 is provided by *Hogan and Brody* [1993]. The major difference between NOGAPS 3.3, which is described by *Hogan and Brody* [1993], and NOGAPS 3.4 is the increase in operational horizontal resolution from T79 to T159. The current operational forecast model is NOGAPS 4.0 (T159L24). This version has undergone a number of changes in the physical parameterizations over NOGAPS 3.4. These changes include a reduction in the ocean surface roughness, based on the work of *Beljaars* [1995], the replacement of the ocean exchange coefficient under stable conditions to the form used in CCM2 [see *Hack et al.,* 1993], and an increase of the stratiform critical relative humidity from 80% to 90% [*Hack et al.,* 1993]. The impact that these changes have on the processes under study here have yet to be fully examined and will be reported in a future study. The resolution of the global spectral forecast component of NOGAPS 3.4 used in this study was T63L18, and the time step was 20 min. The physics package included a bulk-Richardson number-dependent vertical mixing patterned after the European Centre for Medium-Range Weather Forecasting (ECMWF) vertical mixing parameterization [*Louis et al.,* 1982], a time-implicit Louis surface flux parameterization *[Louis,* 1979], gravity wave drag based on *Palmer et al.* [1986], shallow cumulus mixing of moisture, temperature, and winds following *Tiedtke* [1984], a relaxed Arakawa-Schubert cumulus parameterization [*Moorthi and Suarez,* 1992], convective and stratiform cloud parameterization [*Slingo,* 1987], and solar and longwave radiation [*Harshvardhan,* 1987]. Hereinafter, the 3.4 version of the model described above, and used in climate simulation mode in this study, will be referred to as NOGAPS-CL.

The simulation started from initial conditions valid for 00 UT of January 1, 1979, and continued for 17 years. Initial ground wetness was set to climatological values. Sea surface temperature and ice concentrations were interpolated to the current time and Gaussian grid of NOGAPS 3.4 from 1° monthly fields, obtained from Program for Climate Model Diagnosis and Intercomparison. These fields were adjusted to insure that when it is linearly interpolated between monthly average values, the monthly average of the observations is preserved. All average quantities, including net surface longwave and solar radiation, latent and sensible heat release, and cloud quantities were processed as the average monthly sum from each time step of the simulation. At each time step, low, middle, and high clouds were defined as the maximum cloud amounts (convective plus stratiform) in the pressure layers 1000 - 800 mbar, 800 - 400 mbar, and 400 - 1 mbar, respectively.

3. Validation Data

Surface latent and net heat flux data were obtained from the ship-based climatologies of *da Silva et al.* [1994]. While ship-based estimates are known to contain errors on a monthly basis of the order of 40 W m^{-2} or more [*Weare,* 1989], the error for the long-term means is expected to be considerably less (~5-20 W m^{-2}), except in very poorly sampled regions (e.g., southeast Pacific or southern Indian Ocean). Net surface shortwave data sets were obtained from both the *Li et al.* [1993a, b] and the NASA Surface Radiation Budget (SRB) data sets. The former uses top of the atmosphere (TOA) shortwave data from Earth Radiation Budget Experiment (ERBE), along with a simplified transfer model, to compute the net shortwave at the surface from January 1985 to December 1989. The latter uses cloud parameters from the International Cloud Climatology Project [ISCCP; *Rossow and Schiffer,* 1991], along with the

algorithm of *Pinker and Laszlo* [1992], to derive the net surface shortwave flux from July 1983 to December 1990 (see Whitlock et al. [1995] for a description of the data set).

Li et al. [1995] have shown that the values from both these monthly data sets compare quite well to the Global Energy Balance Archive (GEBA) [*Ohmura and Gilgen,* 1991]. This archive contains monthly average surface insolation values from a ground observation network of radiometers with stations throughout Europe, Canada, Russia, Japan, and to some extent Africa, South America, and a few island stations. The Li et al. comparisons showed that the two monthly data sets each agreed with the GEBA observations to within a 10 W m^{-2} bias and a 25 W m^{-2} root-mean-square (rms) difference. In addition, using a set of five in situ buoy records extending over a 2-year period from the tropical/subtropical Atlantic, Waliser et al. [1999c] has shown that the long-term mean errors of these satellite retrievals are likely to be less than about 5 W m^{-2}. Because of the rather good agreement found in the above comparisons between in situ and satellite-derived shortwave values, along with the much better sampling characteristics associated with the latter, we have chosen to use satellite-derived values of surface shortwave instead of the ship-based estimates [e.g. *da Silva et al.,* 1994]. It turns out, however, that the long-term mean ship-derived values [e.g. *da Silva et al.,* 1994; *Josey et al.,* 1999] are actually very similar to the long-term mean satellite-derived quantities (not shown), thus our results are not very sensitive to the choice of data sets. An exception to this rule, however, is the *Oberhuber* [1988] values of net surface shortwave which appear to be an underestimate relative to most other satellite and ship-based retrievals [*Waliser et al.* 1999c].

Validation data for TOA radiation quantities is based on monthly average ERBE data, which extends from January 1985 to December 1989 [*Barkstrom,* 1984; *Hartmann et al.* 1986]. Errors in mean TOA shortwave and longwave quantities are expected to be less than 5 W m^{-2} for long-term regional means. Validation data for precipitation is based on satellite-derived ocean rainfall estimates that employ channels 1-3 of the Microwave Sounding Unit (MSU) [*Spencer,* 1993]. Rain rate is diagnosed when cloud water and rain-water-induced radiometric warming of the channel 1 brightness temperatures exceeds a cumulative frequency distribution threshold of 15% after correction for air mass temperature determined from the channels 2 and 3 measurements. The MSU product used here is a monthly data set that extends from January 1979 to December 1993. Rainfall under any circumstances is hard to measure with a high amount of accuracy. Space-based methods are expected to have an accuracy of about 25% over ocean regions [*Xie and Arkin,* 1997]. While this is a rather qualitative estimate, it is expected that the spatial structures depicted by satellite-based methods are generally realistic. Total columnar water vapor data is based on the SSM/I satellite retrievals of *Ferraro et al.* [1996]. These data cover the period from July 1987 to December 1995, with an 18-month missing period from July 1990 to December 1991. Microwave measurements of total water vapor are one of the most accurate space-borne measurements. Biases associated with long-term means are expected to be a few percent or less.

Cloud frequency data are based on ISCCP C2 data that extend from July 1983 to December 1990 [*Rossow and Schiffer,* 1991]. ISCCP C2 data contain monthly averages of derived cloud types in terms of their frequency of occurrence, cloud top temperatures, and cloud top pressures, along with other auxiliary information. ISCCP C2 distinguishes three cloud levels (low (<800 mbar), middle (> 800 mbar; < 400 mbar); high (> 400 mbar)) based on cloud top temperature (i.e., infra-red) measurements and the associated cloud-top pressure values. Monthly cloud frequencies are computed from the fraction of spatially and temporally subsampled pixels indicating the particular cloud type over an equal-area grid box. The size of the satellite pixels range between about 4-8 km for nadir viewing, growing to tens of kilometers at the scan edges. The equal-area grid box has a 2.5^{o} resolution at the equator. The typical temporal subsampling interval is 3 hours, while the spatial subsampling interval is about 25 to 30 km at nadir. Thus the cloud frequencies from ISCCP are a space and time subsampled statistic of all the pixels measured in a given month in a given equal-area grid box. It is difficult to assign a measurement error for cloud frequencies as it might apply to model comparisons since satellite-estimated clouds and model-diagnosed clouds (see section 2) are not exactly the same quantity nor are they sampled the same way [e.g., *Weare and Mohkov,* 1995]. For this reason we rely on observed cloud data only loosely. The interpretation of model-data differences in clouds is primarily used in this study as additional supporting evidence for the conclusions drawn from the more robustly measured and/or more readily comparable quantities discussed above.

Estimates of the observed large-scale circulation are obtained from the National Centers for Environmental Prediction/National Center for Atmospheric Research (NCEP/NCAR) reanalysis [*Kalnay et al.,* 1996]. Note that NCEP/NCAR categorizes reanalysis variables with the letters A, B, and C, which indicate the degree the variables are influenced by observations versus model physics. "A" variables are strongly influenced by the observations and make up the most reliable category, especially away from the surface. The "A" category includes only zonal and meridional winds, temperature, and geopotential heights. "C" variables are those that have no observations directly affecting them and thus are exclusively model derived, while "B" variables lie in between the "A" and the "C" extremes. We have intentionally restricted our use of reanalysis data to only use relevant fields from the "A" class in order to reduce the chances of comparing the NOGAPS-CL model to another model, rather than to observations, which is our intention. For these reasons we only include comparisons to zonal and meridional winds and 200-mbar velocity potential. In addition, we use the wind stress estimates of *da Silva et al.* [1994] to describe the biases in the strength and structure of the circulation near the surface where the reanalysis product may be more suspect.

For each of the global model-data comparisons discussed in section 4, overlapping months between the model simulation and the validating data were used, except in the case of the comparisons made to the ship-based climatologies (i.e. latent, net heat, and momentum fluxes) where the model climatology, based on the entire simulation, was used.

4. Results

4.1. Surface Fluxes

Figure 1 is a comparison of the long-term mean net (downward-upward) surface shortwave field between the

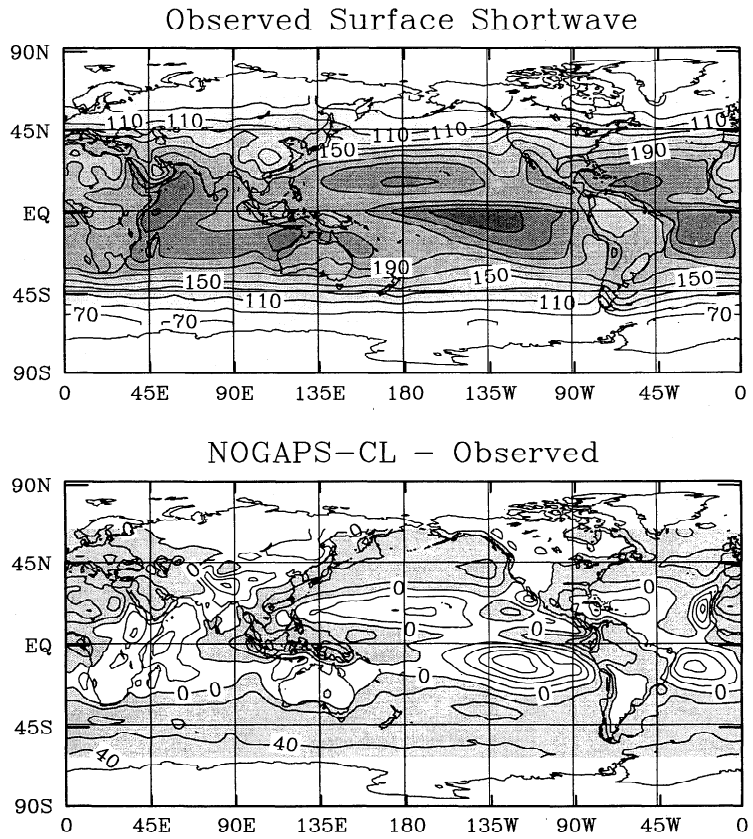

Figure 1. (top) Long-term mean satellite-derived net surface shortwave radiation from *Li et al.* [1993a, b]. (bottom) Difference between NOGAPS-CL-simulated net surface shortwave radiation and the satellite-derived values (see section 2 for NOGAPS-CL definition). Data period used for both plots is January 1985 to December 1989. Contour intervals are 20 W m^{-2}.

NOGAPS-CL simulation and the satellite-derived shortwave product of *Li et al.* [1993a, b] for the overlapping months of the two data sets (i.e., 60 months). Most evident are the negative biases (< -40 W m^{-2}) which occur in the north central and southeast Pacific, northwest and southwest Atlantic, and western Indian Oceans. These biases indicate that too little solar energy is being transmitted to the ocean. Positive biases are evident in other regions, including the western equatorial Pacific and midlatitude oceans, indicating that too much solar energy is being transmitted to the oceans in these areas. The long-term mean shortwave retrievals from the NASA SRB data set [i.e., *Pinker et al.,* 1992] have a similar spatial structure to the *Li et al.* [1993a, b] data shown in Figure 1 but with a slightly greater magnitude (about 10%). Thus in comparison to NOGAPS-CL, the negative (positive) biases are slightly larger (smaller). A comparison to the bulk parameterized net shortwave of *da Silva et al.* [1994] also showed very similar results, with the main difference being that the positive bias near the maritime continent was about 10 W m^{-2} weaker.

While the biases in surface shortwave flux indicate a large error for the long-term surface energy budget, often such climate model biases are offset by biases in other components of the heat budget (e.g., latent heat flux [*Ma et al.*, 1994; *Zhang*, 1996]). This does not appear to be the case for the NOGAPS-CL simulation. Figure 2 compares the long-term mean latent heat flux from *da Silva et al.* [1994] and the NOGAPS-CL model and shows that in many of the same, or nearby, areas that have too little solar energy entering the ocean, there is also too much latent heat loss from the ocean. Specifically, in most of the subtropics the NOGAPS-CL surface latent heat flux is biased high by about 10 to 70 W m^{-2}. This systematic error appears to be a common feature in many climate-modeling systems [*Gleckler and Weare,* 1997]. In addition to the positive latent heat flux biases in the subtropics, NOGAPS-CL appears to exhibit negative latent heat flux biases of a similar magnitude over the North Pacific and Atlantic western boundary currents and under the storm track regions extending eastward from them. The boundary current regions tend to exhibit the highest observed mean heat fluxes (top panel) due to the advection of relatively cold and dry air over the underlying warm western boundary currents (e.g., Gulf Stream). Comparison of the climatological latent heat flux from the *Josey et al.* [1999] data set to the NOGAPS-CL long-term mean latent heat flux (not shown) indicates nearly identical results, and thus the magnitudes and spatial structure of these biases do not appear to be data set dependent.

Since both the shortwave and the latent heat flux biases imply too little energy entering the ocean in much of the tropical/subtropical regions, it is not surprising to see sizeable negative biases in these same areas in the comparison of net surface heat flux shown in Figure 3. Typical errors in the subtropical regions are of the order of -30 to -70 W m^{-2}, with biases in the midlatitude regions having the opposite sign but a similar magnitude. Note that

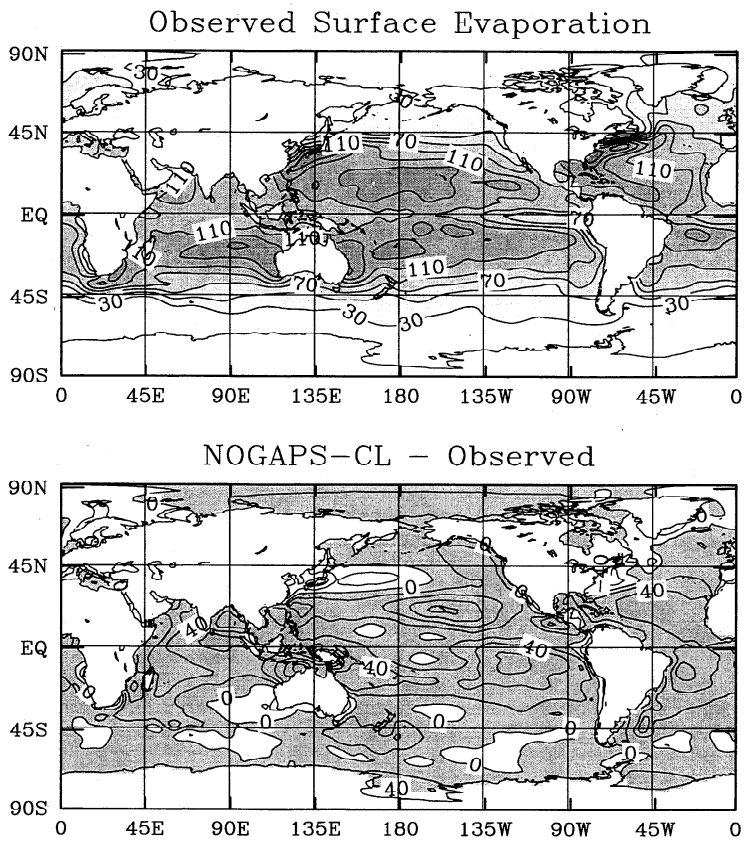

Figure 2. (top) Long-term mean ship-derived surface latent heat flux from *da Silva et al.* [1994] climatology. (bottom) Difference between NOGAPS-CL-simulated surface latent heat flux and the ship-derived values. Data period used for the model long-term mean includes the entire 17 years of simulation. Contour intervals are 20 W m^{-2}.

the structure of these errors is fairly similar to that in the uncoupled Hadley Centre model shown by Meehl's [1997] analysis of surface flux errors in component versus coupled GCMs. While neither the magnitude nor the structure of these errors is expected to remain the same upon coupling, Meehl's analysis suggests that they will still very likely contribute to significant errors in sea surface temperature (SST) upon coupling to an ocean model (assuming no flux correction). On the basis of analyses such as Meehl's and the suggestion by *Rosmond* [1992] that 10 W m^{-2} is an acceptable bias in the net heat flux for a coupled modeling system, these errors represent a remaining challenge to overcome with respect to undertaking long-term (e.g., seasonal) coupled ocean simulations and predictions.

Apart from the shortcomings with the data sets used for "validation" (see section 3), the combined information provided by the shortwave and latent heat flux comparisons suggests that the biases associated with the shortwave flux stem from factors other than, or at least in addition to, the parameterization of radiation. The similar size errors found in the latent heat flux, which is closely tied to the hydrological cycle, are likely to be contributing to problems in the convection and cloud fields. Thus the underlying uncertainty in the shortwave may have little to do with the parameterization of the shortwave radiation and its interactions with clouds; it may instead be a problem with the parameterization of the cloud field and thus represent a highly coupled problem involving surface fluxes, convection, dynamics, etc. In the following sections we examine additional model-observation comparisons of related quantities to ascertain the possible mechanism(s) behind the shortwave and latent flux biases described above.

4.2. TOA Absorbed Solar

Given the biases in the surface shortwave described above, it is of interest to determine their relationship to biases at the top of the atmosphere. By examining the solar radiation budget at the top of the atmosphere, we can determine if the shortwave bias occurs in the clear or cloudy sky. Figure 4 shows the long-term mean differences in the clear-sky absorbed solar energy at the top of the atmosphere (TOA) between the ERBE-derived observations and the NOGAPS-CL simulation. Evident is the fact that there is little or no model-observation bias, especially over the oceans (< 7 W m^{-2}). This indicates that the shortwave bias at the ocean surface does not appear to stem from a problem in the parameterization or simulation of clear-sky shortwave radiation. However, since the model-data discrepancies we are addressing stem from shortwave comparisons at the surface, it would be prudent to have an independent check of the modeled net clear-sky shortwave at the surface. This was accomplished by comparing the net surface shortwave values from the NOGAPS-CL radiation scheme to that computed by the radiation model [*Briegleb,* 1992] from the National

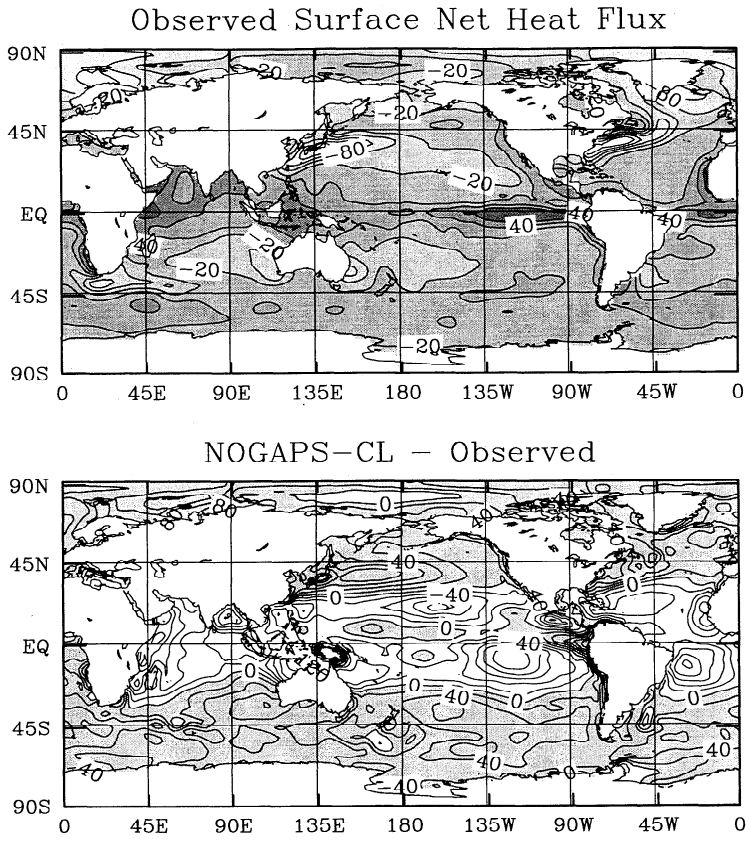

Figure 3. (top) Long-term mean ship-derived surface net heat flux from da Silva et al. [1994] climatology. Contour intervals are 30 W m^{-2}. (bottom) Difference between NOGAPS-CL-simulated surface net heat flux and the ship-derived values. Contour intervals are 30 W m^{-2}. Data period used for the model long-term mean includes the entire 17 years of simulation.

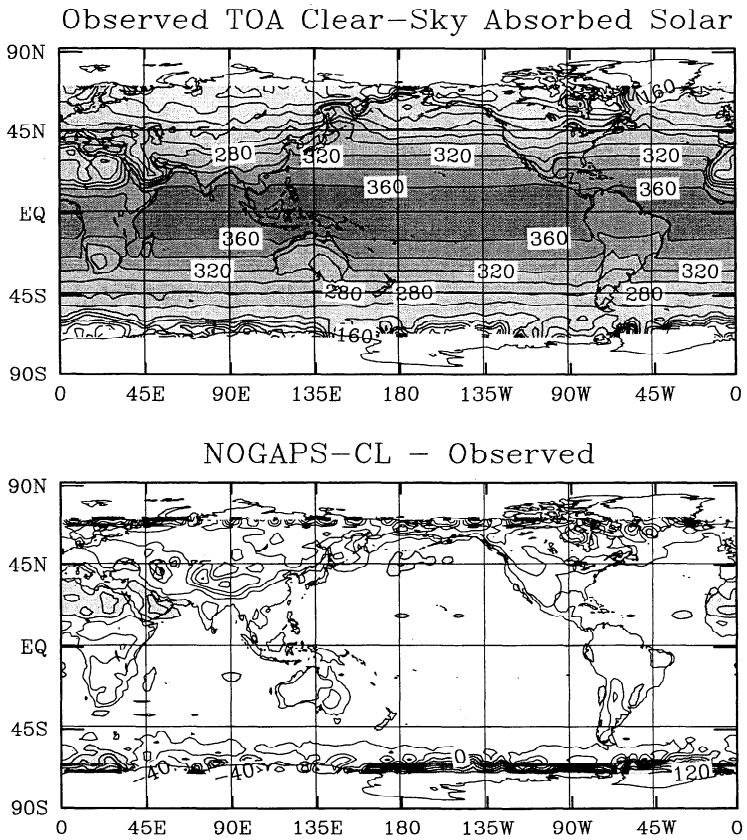

Figure 4. (top) Long-term mean satellite-derived clear-sky absorbed solar radiation from Earth Radiation Budget Experiment (ERBE). (bottom) Difference between NOGAPS-CL-simulated values and the ERBE-derived values. Data period used for both plots is January 1985 to December 1989. Contour intervals are 20 W m^{-2}.

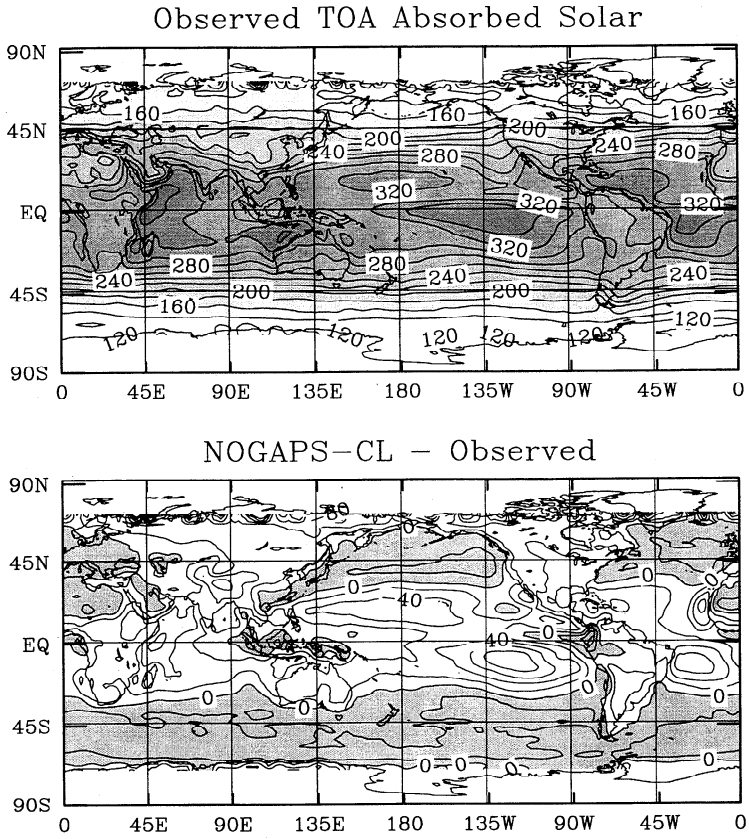

Figure 5. Same as Figure 4 except for all-sky absorbed solar radiation.

Center for Atmospheric Research (NCAR) Community Climate Model Version 3 (hereinafter referred to as CCM3) [*Kiehl et al.*, 1998]. The CCM3 clear-sky computations have been validated with a number of in-situ data sets [e.g., *Zender et al.*, 1997; *Jing and Cess,* 1998; *Waliser et al.* 1999c], and therefore it provides a fairly robust benchmark to verify the NOGAPS-CL net shortwave flux computations.

A model-to-model clear-sky comparison was performed by computing the daily-averaged net surface shortwave flux with both models for the first day of each month for a calendar year, for grid points spaced 10° in longitude and 5° in latitude from 30°N to 30°S and 100°E to 260°E (i.e., most of the tropical Pacific Ocean). The daily-averaged values were estimated from calculations performed every hour. The resulting 2652 daily-average values have a mean rms difference of about 0.5 W m^{-2} and a mean bias of 0.4 W m^{-2} (NOGAPS-CL being higher). Thus the clear-sky agreements with ERBE at the TOA and with another well-verified model at the surface indicate that the problem observed in the surface shortwave is likely to stem from shortcomings associated with the cloudy atmosphere.

Figure 5 shows the long-term mean differences in the "all-sky" absorbed solar energy at the TOA between the ERBE observations and the NOGAPS-CL model. In this case it is very evident that the negative biases in this figure (i.e., too little solar energy being absorbed by the atmosphere-ocean system) have a close relationship to the negative biases seen in the surface shortwave shown in Figure 1. Further, since the problem was not evident in the clear sky (Figure 4), it is apparent that the large negative surface shortwave biases result from either too many clouds or clouds that are too reflective. At this point it would be useful to be able to perform a model-to-model comparison for the cloudy sky such as the one described above for the clear sky. This might help to pin down, for example, if the modeled clouds are too reflective. Unfortunately, there is no well-verified radiation scheme for the cloudy atmosphere to use as a benchmark. Even more relevant, however, is the fact that the procedure for even attempting such a model-to-model comparison for cloudy skies is very difficult due to the different ways clouds are parameterized and input into GCM radiation models.

Fouquart et al. [1991] attempted a multimodel shortwave comparison as part of the Intercomparison of Radiation Codes Used in Climate Models (ICRCCM) study. The study examined the variations between 26 schemes, one of which was the *Harshvardhan et al.* [1987] scheme, for two different cloudy atmospheres. They found the disagreement amongst the different codes to lie between about 4 and 10%, with larger disagreement for cloudier skies. Beyond these results, the authors reported difficulty in determining the underlying causes for the model-to-model discrepancies mostly due to the heterogeneous nature of the different radiation schemes being examined and the lack of availability and quality of crucial input and validation data. Relevant at least to the present study was the finding that the *Harshvardhan et al.* [1987] scheme did not represent an outlier among the models studied (V. Ramaswamy, personal communication, 1999). On the basis of this finding, it is then likely that much of the negative biases in the shortwave flux at the surface and the TOA in the tropical regions may, to first order, result from too many clouds, rather than the modeled

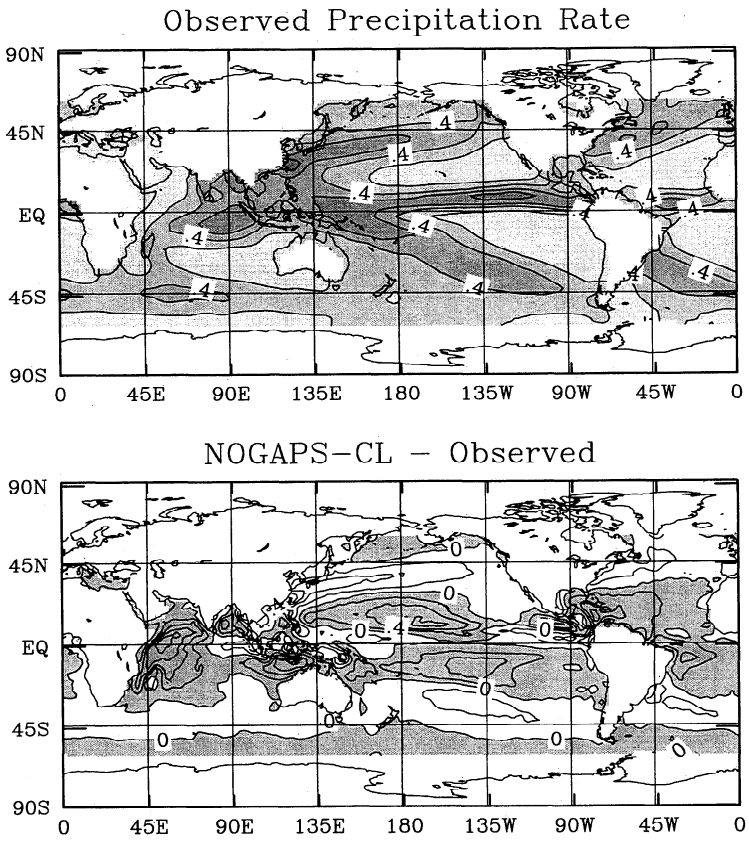

Figure 6. (top) Long-term mean satellite-derived precipitation rate from Microwave Sounding Unit (MSU) [*Spencer,* 1993]. (bottom) Difference between NOGAPS-CL-simulated values and the MSU-derived values. Data period used for both plots is January 1979 to December 1993. Contour intervals are 0.2 cm d^{-1}.

clouds being modeled as too reflective. To examine this possibility, we will proceed with comparisons between modeled and observed precipitation and outgoing longwave radiation (OLR), each of which provides relevant information on the distributions of cloudiness. The virtue of starting with these quantities is that they are fairly well measured quantities, especially the OLR, and even more importantly, each is perfectly compatible with model-derived quantities. Once we have a more complete physical description of the model biases from these comparisons, we will proceed to examine the agreement between modeled and observed cloud fractions (a more tenuous comparison; see section 3) to determine if the description is further supported by the cloud comparisons.

4.3. Precipitation

The comparison of the long-term mean NOGAPS-CL precipitation to the MSU-derived estimate is shown in Figure 6. Positive biases ranging from 0.1 to 0.6 cm d^{-1} occur in the subtropics near the edges of the deep convective regions. The global structure of this precipitation bias shows considerable similarities to the bias of the ensemble mean of the AMIP I models reported by *Lau et al.* [1996], and thus to some extent the precipitation biases exhibited in this simulation appear to be common among many GCM climate simulations. Furthermore, the spatial structure of the positive precipitation bias shown in Figure 6 appears to have a somewhat systematic relation to the biases exhibited by the latent heat flux (Figure 2). In particular, most of the maxima associated with the latent heat flux bias in the trade wind regions tend to form slightly "upwind" of the precipitation bias maxima, which are themselves "upwind" from the zones of very deep convection. The relationship between these two fields will be discussed in more detail in section 4.6. (It is worth noting that while the enhanced evaporation discussed in section 4.3 will increase the freshwater flux out of the ocean (50 W m^{-2} ~ 0.2 cm d^{-1}), the enhanced rainfall in nearby overlapping areas will decrease it by a similar amount. Thus in some regions the biases in the freshwater fluxes are reduced due to the close proximity of bias maxima in evaporation and precipitation (e.g., north and south central tropical Pacific, western Indian Ocean).)

Regarding the earlier supposition concerning cloudiness, the spatial structure of the precipitation bias helps support the idea that there may, in fact, be too much climatological cloudiness in the areas of negative shortwave bias. In most subtropical regions where there is significant negative surface shortwave bias, there is also a positive rainfall bias (except in the far eastern portions of Pacific and Atlantic where both the climate simulation and the observations exhibit almost zero rainfall, e.g., southeast Pacific). In addition, the area in the western Pacific warm pool, which exhibits a positive surface shortwave bias, also displays a negative precipitation bias. Again, these precipitation comparisons indicate that the shortwave problem is not, or not just, a radiometric problem concerning

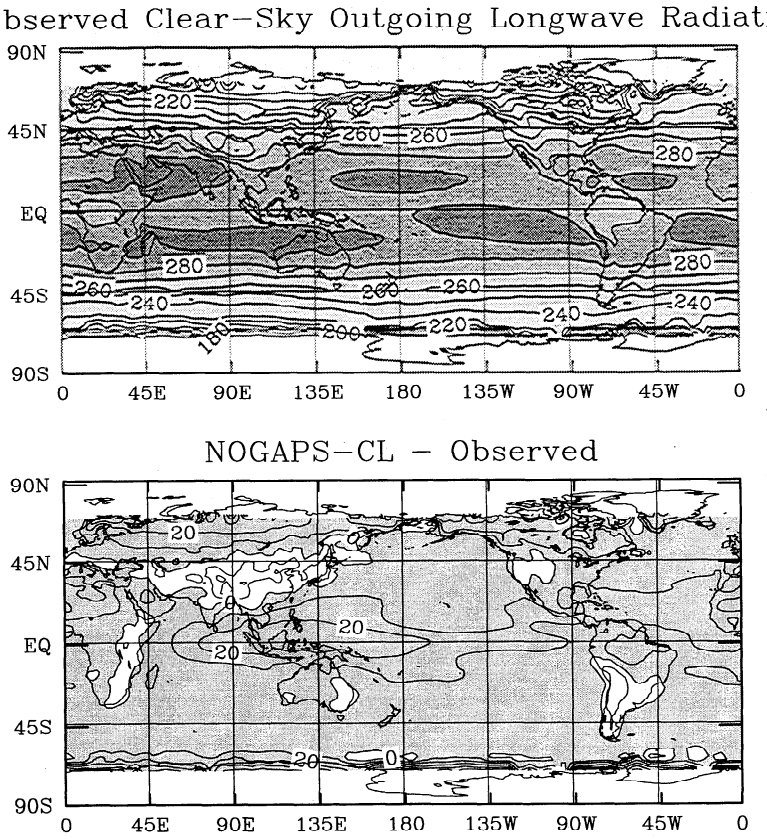

Figure 7. (top) Long-term mean satellite-derived clear-sky outgoing longwave radiation from ERBE. (bottom) Difference between NOGAPS-CL-simulated values and the ERBE-derived values. Data period used for both plots is January 1985 to December 1989. Contour intervals are 10 W m^{-2}.

the parameterization of radiation for a given cloud field but an indication that the NOGAPS-CL simulation has too many clouds in the subtropics and too few clouds in the warm-pool region of the western Pacific. Furthermore, it is worth highlighting that the precipitation biases discussed in this subsection must inherently be connected to shortcomings in the model's internal latent heating field and associated large-scale circulation, and as indicated above, they also appear to be systematically related to biases in the surface latent heat flux. In the following sections the connections between the biases in precipitation and clouds, surface shortwave and latent heat fluxes, and the large-scale dynamics will be elaborated on further.

4.4. Longwave Radiation and Water Vapor

Examination of the outgoing longwave radiation (OLR) also helps support some of the above suggestions concerning the biases in the cloud structures that seem to underlie the shortwave biases. Figure 7 shows the difference in the TOA clear-sky OLR between the ERBE and the NOGAPS-CL simulation. The figure shows that the modeled values are too high over most of the deep tropical/convective areas. Since this is a clear-sky quantity, it does little in the way of addressing the cloudy-sky differences described above. However, the underlying reason for this bias helps to complete a picture illustrating the mechanism(s) behind the long-term model-data differences in the cloudy-sky quantities, as well as linking these biases with those associated with the surface heat fluxes and large-scale circulation. Figure 8 shows the difference in long-term mean precipitable water between the SSM/I-derived observations and the NOGAPS-CL simulation. Note that in most of the same areas that have too much clear-sky OLR, the atmosphere is too dry. Given that the model simulation was run with observed monthly averaged SSTs, the excess clear-sky OLR emanating from the deep tropics in the climate simulation appears to be due to the negative bias in precipitable water which allows too much OLR to escape from the clear-sky atmosphere. This low bias in precipitable water over the western Pacific is common to many models [*Duvel, et al.,* 1997], and overall, the results from AMIP show that the NOGAPS-CL mean precipitable water over the Pacific basin is very close to the mean of the AMIP models [*Gaffen, et al.,* 1997]. Figure 9 is similar to Figure 7 except it shows the difference in all-sky OLR. This figure indicates that many of the regions that have a negative bias (too little OLR being emitted by the climate model) are the same regions that have a negative bias in surface shortwave. These negative biases in all-sky OLR again suggest that there are too many clouds or, in this case, maybe that the cloud tops are too high. Further, the large region of positive all-sky OLR bias in the warm pool region (~ 40-50 W m^{-2}) cannot be completely accounted for by the clear-sky OLR bias (~ 25 W m^{-2}, Figure 7), suggesting that in this region the NOGAPS-CL exhibits too few clouds or that its cloud tops are too low. These warm-pool OLR biases are consistent with the collocated positive biases in the surface

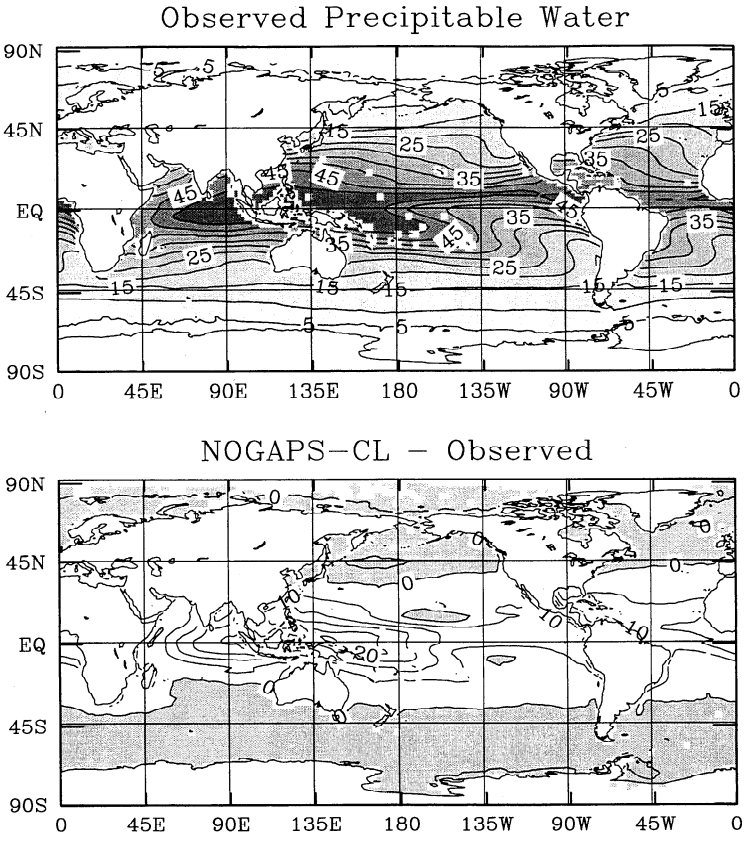

Figure 8. (top) Long-term mean satellite-derived precipitable water from Special Sensor Microwave Imager (SSM/I) [*Ferraro et al.*, 1996]. (bottom) Difference between NOGAPS-CL-simulated values and the SSM/I-derived values. Data period used for both plots is January 1987 to December 1995. Contour intervals are 5 mm.

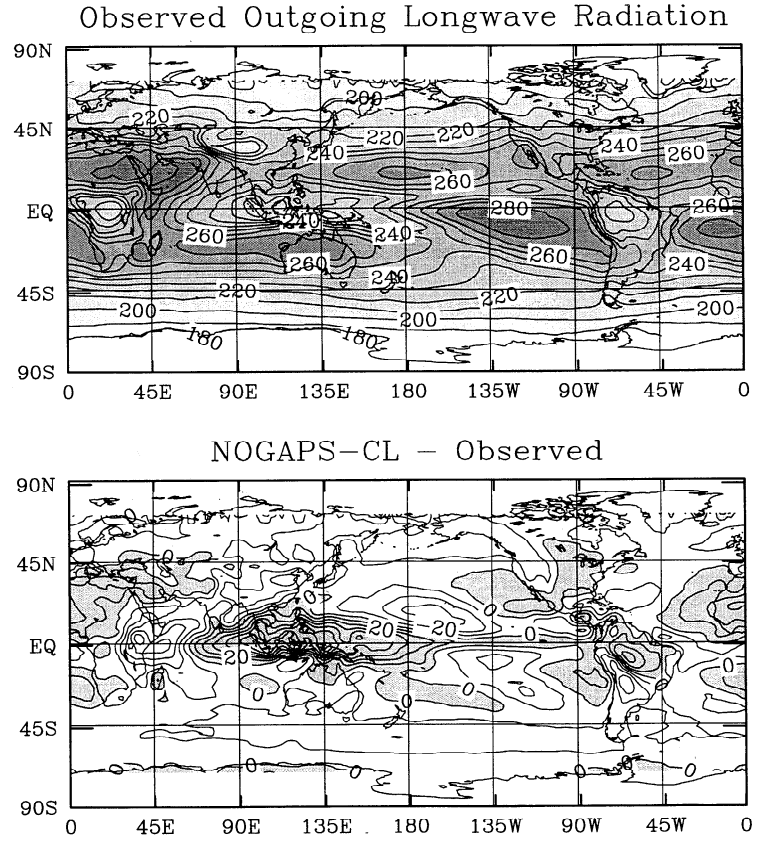

Figure 9. Same as Figure 7 except for all-sky outgoing longwave radiation. Contour intervals are 10 W m^{-2}.

shortwave (Figure 1) and all-sky absorbed solar (Figure 5) and the negative biases in precipitation (Figure 6).

4.5. Cloud Amounts and Types

The results and discussion above points to the likelihood that the NOGAPS-CL simulation exhibits too many clouds and/or clouds that are too bright or too high in regions having a negative shortwave bias at the surface (i.e., southeast and north central Pacific) and too few clouds and/or clouds that are too dark or too low in regions having a positive shortwave bias (i.e., regions that are strongly deep convective, such as the warm pool). Examination of the model biases in the cloud structure helps to support these suggestions. Figure 10 shows a comparison between total cloud frequency from ISCCP and the NOGAPS-CL simulation. Note that it is difficult to compare model and observed cloud fractions/frequencies since they are not measured in exactly the same way (see Sections 2 and 3). For example, the zero bias in Figure 10 and in Figures 11-13 may not represent the true zero model bias in the simulated cloud amount relative to observations due to the differences in the way these quantities are represented/measured. Therefore we will tend to focus on the spatial structures of the cloud-frequency biases rather than on their absolute values with the intention of using these comparisons primarily to support or refute the suggestions derived from the previous comparisons (e.g., shortwave fluxes, precipitation, OLR, etc.).

The total cloud comparison in Figure 10 indicates relatively too many clouds in the southeast and possibly the north central Pacific and too few clouds in the warm-pool region and midlatitude regions, both of which are roughly consistent with the indirect evidence provided in the other comparisons described above. To help illustrate the type(s) of clouds contributing to these biases, Figures 11, 12, and 13 show comparisons between ISCCP and model-simulated high-, middle-, and low-cloud amounts, respectively. These figures suggest that the model produces too few high (or deep) clouds in the warm-pool region and too many clouds, mainly high- and middle-level clouds, in many of the regions that have a negative shortwave bias. Thus even though the model-data cloud comparisons have to be viewed with some caution, they tend to support the suppositions regarding "cloudiness" from the other, more well posed, comparisons presented above. While our focus has primarily been in the tropics where the largest biases are evident, Figure 13 also indicates that the positive surface shortwave bias in the midlatitudes might be, at least in part, due to too few low clouds in these regions. In section 4.6, we will draw the results of all of the above comparisons together to help assess the underlying shortcoming(s) in the model that may be contributing to the biases in the surface heat fluxes.

4.6. Discussion and Hypothesis

The depiction of the NOGAPS-CL mean climate biases in the fields described above suggests a problem with the way clouds are produced/diagnosed. The model-data comparisons of the shortwave quantities at the surface and TOA indicates that the clouds are either too bright or occur

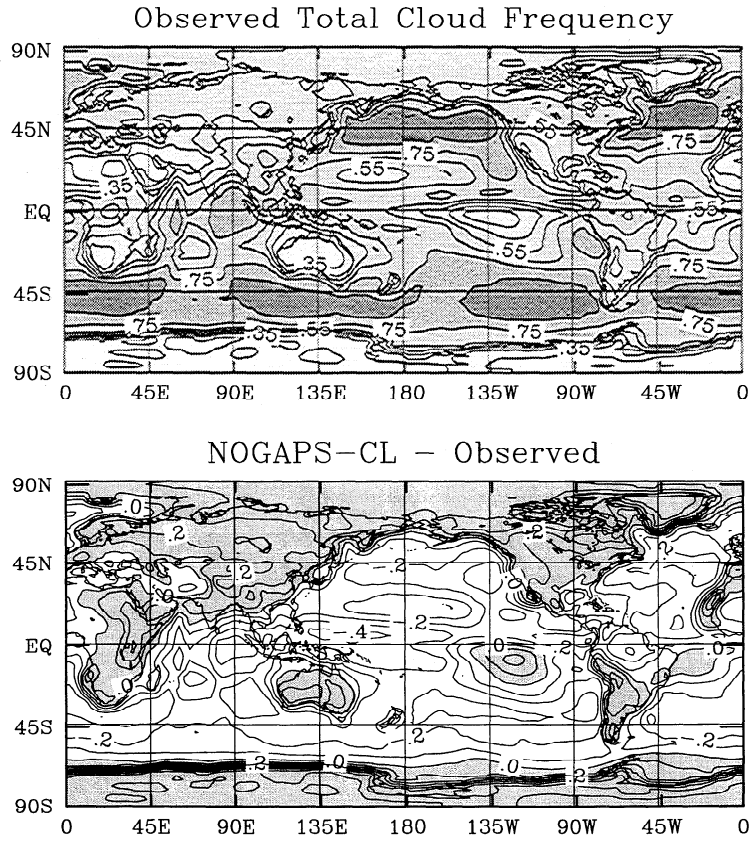

Figure 10. (top) Long-term mean satellite-derived total cloud frequency from International Satellite Cloud Climatology Project (ISCCP). (bottom) Difference between NOGAPS-CL-simulated values and the ISCCP-derived values. Data period used for both plots is July 1993 to December 1990. Contour intervals are 0.1.

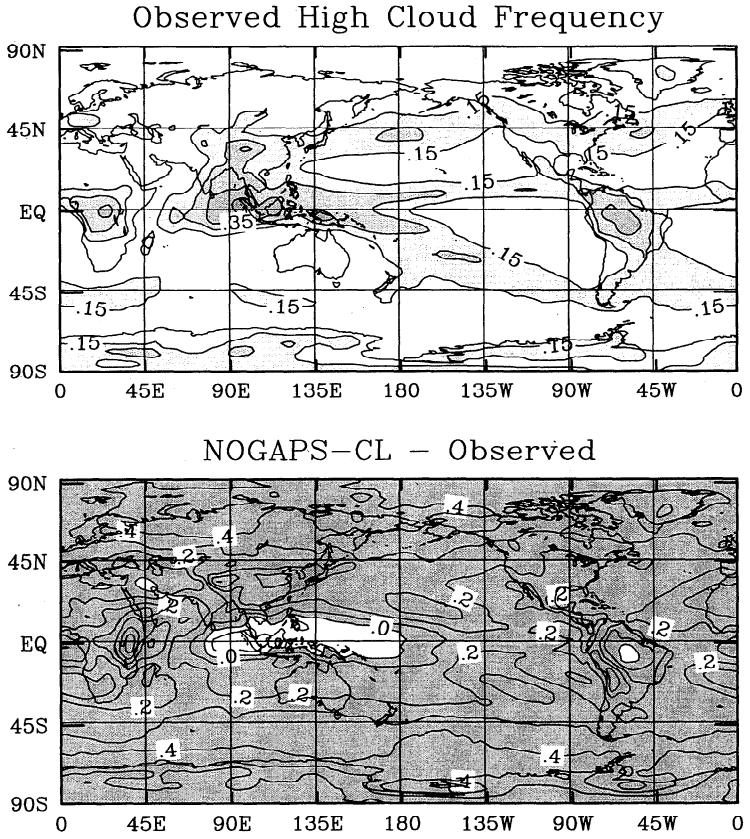

Figure 11. Same as Figure 10 except for high cloud frequency.

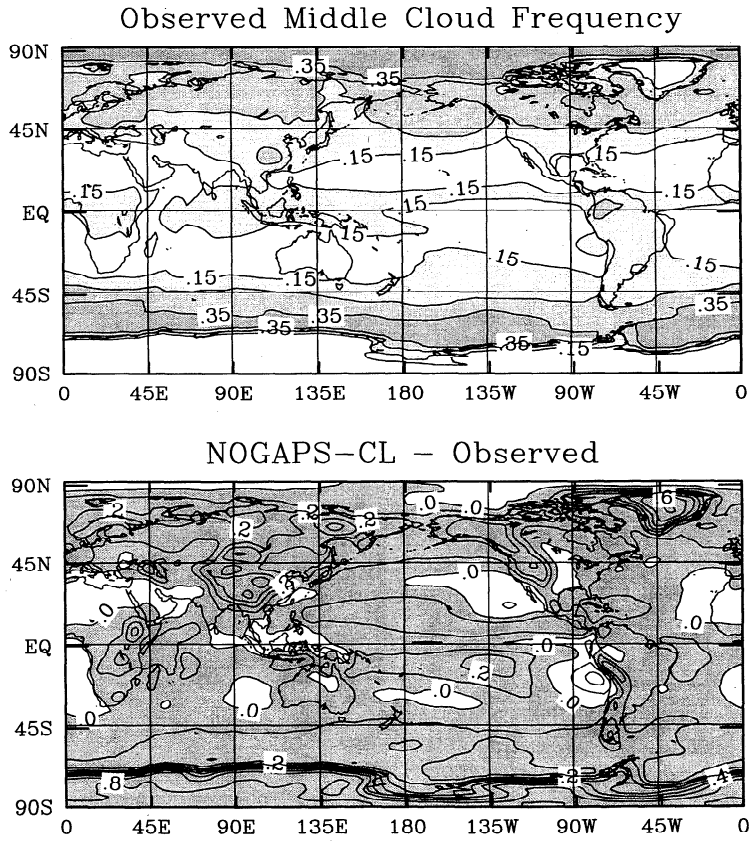

Figure 12. Same as Figure 10 except for middle cloud frequency.

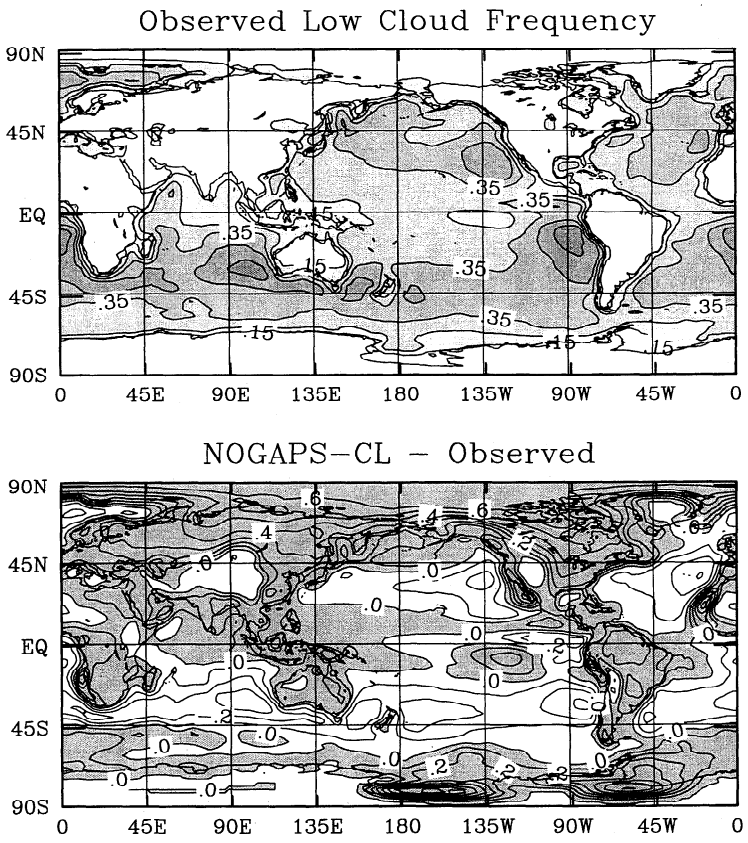

Figure 13. Same as Figure 10 except for low cloud frequency.

too frequently in areas near the edges of tropical deep convective zones. The model-to-model radiation comparisons in addition to the model-data comparisons of rainfall, all-sky OLR, and cloud amounts all indicate that this problem extends well beyond a radiometric problem (i.e., too bright of clouds) but indeed involves clouds that occur too frequently. Such a shortcoming might arise from a deficiency in the NOGAPS-CL parameterization of convective or stratiform precipitation. Given the bulk of the problem concerning the radiation biases occurs in the tropics, where the rainfall is almost exclusively derived from the cumulus processes, it is more likely related to the former.

Figure 14 shows a schematic representation that attempts to tie the above climate biases together. The upper diagram shows a representation of the "observed" atmosphere. The diagram depicts air moving equatorward (or westward toward the warm pool) to warmer and warmer sea surface temperatures (SSTs). As it progresses, the air moistens through local latent heat flux. A portion of this moisture is removed via local vertical instability (i.e., convective rainfall and cloud top detrainment), but a significant amount is transported via large-scale convergence to the warmest, most convective regions of the tropics. The ensuing deep convective rainfall in these areas produces a strong upper level circulation that in turn helps suppress the weaker convection in the subtropical areas through subsidence and associated dry-air entrainment. The bottom diagram shows a representation of the NOGAPS-CL atmosphere. In this case, convection occurs too frequently/readily in regions adjacent to the observed deep convection zones where the SST is cooler. This leads to a concomitant increase in the local cloudiness and rainfall and a decrease in the surface shortwave and all-sky OLR, as well as an increase in evaporation in regions adjacent but "upwind" of the enhanced convection. Because the convective instability is released too early, not enough water vapor is transported to the warmest and most deep-convective areas leaving the atmosphere in this region too dry. The early release of the instability also means that there are too few clouds (and/or clouds that are too low), too little rain, and too much OLR and surface shortwave in the warmest regions. Overall, the lack of deep convection in the areas of warmest SST, as well as the reduction in longwave radiation trapping, reduces the strength of the climatological large-scale circulation, which in turn does not produce the needed subsidence in the subtropical areas to help suppress the local instability.

Figure 15 provides an indication of how the biases in convection (i.e. rainfall) impact the surface wind field and lead to the model biases in the surface evaporation. The top plot shows the long-term mean surface wind stress over the Pacific Ocean [*da Silva et al.* 1994] along with an indication (see caption) of the regions of maximum precipitation (thick dashed line) and evaporation (thin solid line). As expected, the maxima in precipitation generally occur where the wind vectors indicate convergence, while the maxima in evaporation lie just outside these regions (i.e., "upwind") where the surface wind field tends to be stronger (and also, of course, where the air mixing into the boundary layer from above tends to be consistently drier). The bottom plot is analogous to the top except that it displays the model biases

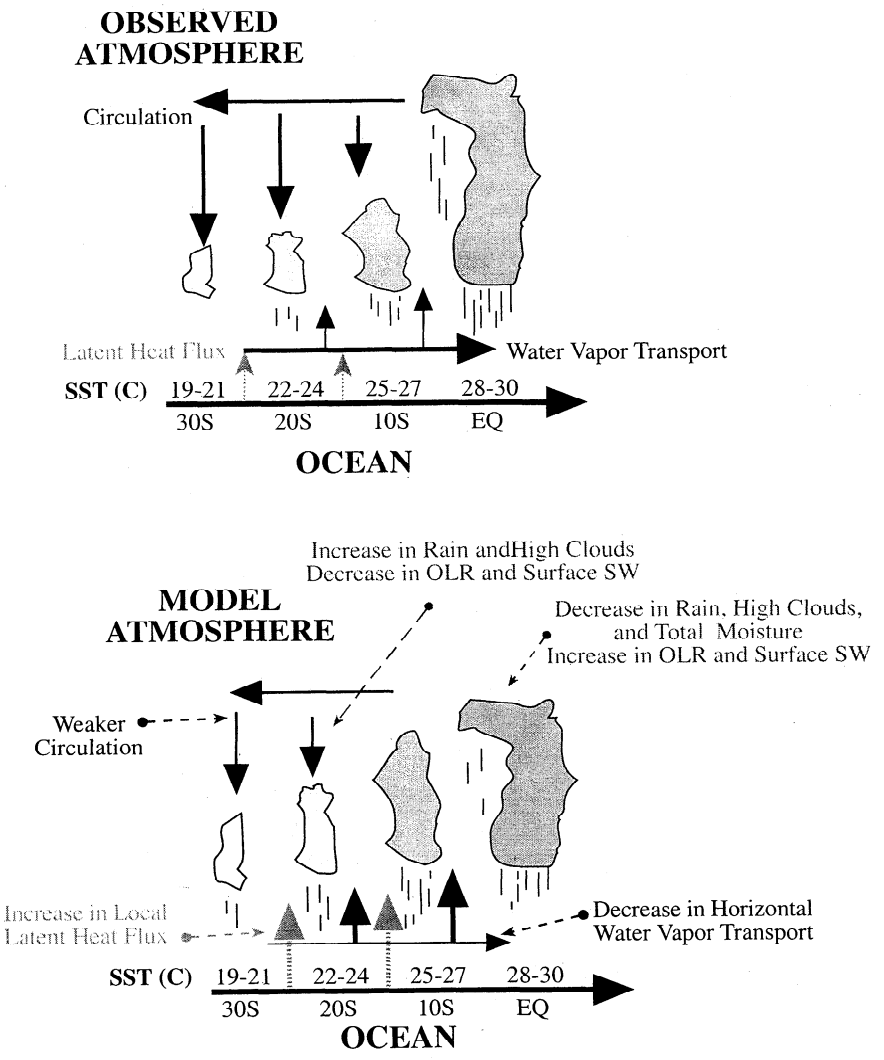

Figure 14. Schematic depiction of coupling between surface fluxes, hydrological cycle, and dynamic processes in the observed atmosphere (top) and the NOGAPS-CL simulation (bottom). Solid arrows indicate processes or features, while dashed arrows with circles indicate errors in processes or features.

in these same fields. Consistent with the discussion above and the associated schematic is an indication of the "early" release of moist instability in areas lying just outside the observed deep convection zones (i.e., thick dashed line). Furthermore, just as the mean winds and evaporation are strongest just outside the observed deep convection zones, the positive biases in evaporation (thin solid line) are found "upwind" of the precipitation biases, particularly in regions where the wind stress biases lead to increases in the mean wind stress (e.g., north central Pacific but not equatorial central Pacific). The plots in this figure help to demonstrate how the NOGAPS-CL biases in surface evaporation result, at least in part, from the biases in rainfall, which in the tropics in this model is almost entirely associated with the convective parameterization (not shown).

Additional support regarding the weakened large-scale circulation discussed above and highlighted in the schematic is presented in Figure 16 which shows the long-term mean 200 mbar velocity potential from the NCEP/NCAR reanalysis [*Kalnay et al.*, 1996] and the NOGAPS-CL simulation. Evident is the stronger, more concentrated region of divergent circulation over the western Pacific in the reanalysis as compared to the NOGAPS-CL values. The weaker and more diffuse velocity potential minimum in the NOGAPS-CL field implies a weaker large-scale tropical circulation (i.e., Hadley and Walker circulations) for the NOGAPS-CL simulation and thus a reduction in subsidence in regions outside the tropical deep convective areas. Since the divergent component of the wind is dependent on the atmospheric diabatic heating and thus the NCEP/NCAR model physics, there is some uncertainty associated with the above comparison and associated validation "data."

Figure 17 shows a direct comparison of winds between NOGAPS-CL and the reanalysis; note that middle and upper level winds tend to be one of the more robust quantities produced by the reanalysis (see section 3). This figure provides some insight into the strengths of the local meridional (i.e., Hadley) and zonal (i.e., Walker) large-scale circulations associated with the deep heating region overlying the maritime continent. The top two panels compare the zonal wind averaged between 15°N and 15°S. While there is some evidence for a weakened eastward flow in

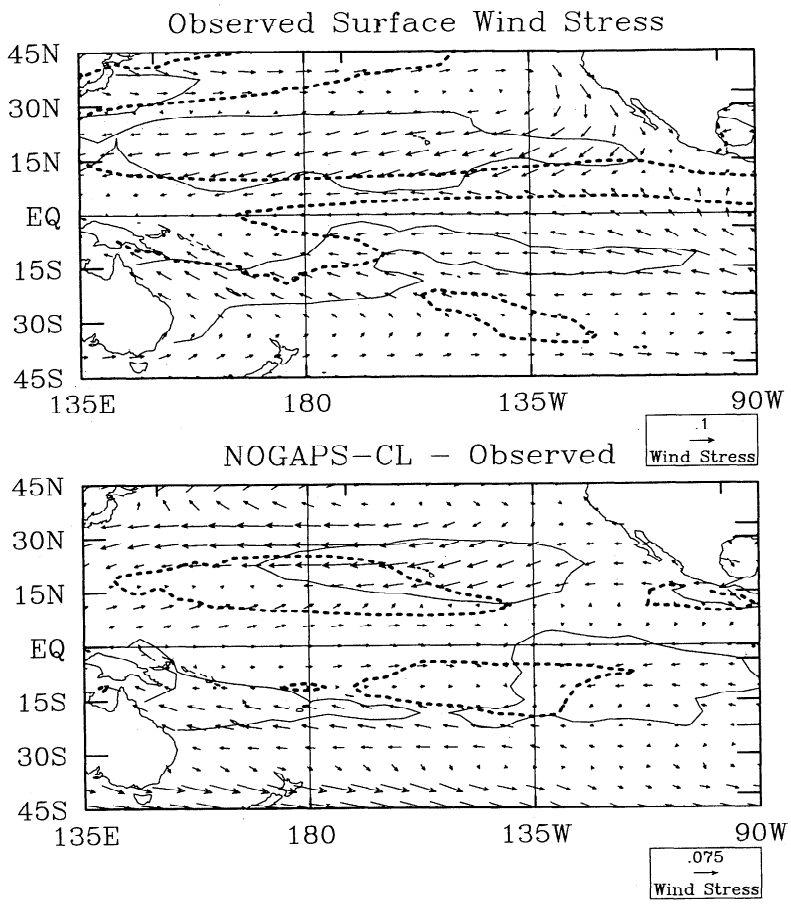

Figure 15. (top) Long-term mean ship-derived surface wind stress from *da Silva et al.* [1994] climatology. (bottom) Difference between NOGAPS-CL-simulated surface wind stress and the ship-derived values. Units are N m^{-2}. Data period used for the model long-term mean includes the entire 17 years of simulation. The thin solid contours are the 125 W m^{-2} (top) and +40 W m^{-2} (bottom) levels from the corresponding evaporation comparisons in Figure 2. The thick dashed contours are the 0.5 cm d^{-1} (top) and +0.3 cm d^{-1} (bottom) levels from the corresponding precipitation comparisons in Figure 6.

the NOGAPS-CL simulation compared to the reanalysis at low and mid levels over the Indian Ocean, the starkest difference is in the much weaker upper-level response in the NOGAPS-CL simulation to the east of the heating region, i.e., the region of the tropics most closely associated with the Walker circulation. This difference is worth considering in light of the theoretical analysis of *Gill* [1980] who showed that the response of the tropical atmosphere to deep tropospheric heating located on the equator consisted primarily of a damped Kelvin wave extending east along the equator and a damped symmetric Rossby wave extending to the west. From Gill's results it is not surprising that most of the difference in the equatorial zonal wind field between NOGAPS-CL and the reanalysis is found over the Pacific Ocean given the differences observed in the equatorial heating patterns (Figures 6,7, and 9). The bottom two panels compare the meridional wind averaged between 60°E and 120°E for NOGAPS-CL and the reanalysis. This longitude range was chosen to highlight the region of the atmosphere that should exhibit the Rossby wave portion of the response associated with a difference in deep equatorial heating. As with the zonal winds, the upper level circulation in the NOGAPS-CL simulation is much weaker than the reanalysis, with the latter depicting a more classical "Hadley"-type circulation [cf., *Waliser et al.*, 1999c].

Further evidence for the scenario described above comes from the distributions of rainfall versus SST shown in Figure 18. The thick and thin lines in the figure shows the distributions of total rainfall versus SST for the region 30°N to 30°S for the years 1979-1988 from the NOGAPS-CL simulation and the MSU observations, respectively. The dashed line indicates the number of values in each SST bin. While specific magnitudes between these two quantities might be hard to compare directly given the uncertainties in the validating quantity, their shapes should be roughly equivalent. However, the NOGAPS-CL simulation shows two significant peaks, one at 28°C and one at 31°C, while the MSU-derived rain rate shows only one peak at about 29.5°C. The latter is consistent with a number of other observed rainfall proxies [*Waliser and Graham,* 1993, Figure 1]. Considering these data in conjunction with the number of values in each bin (dashed), the peak at 28°C is the value at which most of the rainfall is occurring and most of the vertical instability is being released. This value is about 1°-1.5°C cooler than the equivalent quantity for the observations. This is qualitatively similar to the schematic in Figure 14 and

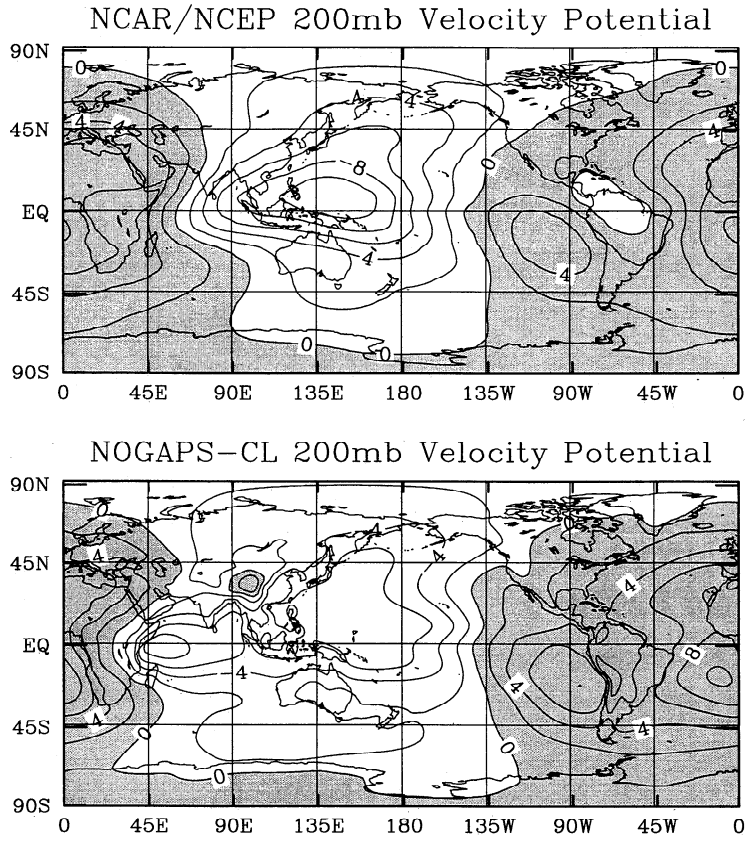

Figure 16. Long-term mean 200 mbar velocity potential from National Centers for Environmental Prediction/National Center for Atmospheric Research (NCEP/NCAR) reanalysis (top) and from the NOGAPS-CL simulation (bottom). Data period used for both plots is January 1979 to December 1995. Contour intervals are 2.0 x 10^6 m^2 s^{-2}.

suggests that too much moist instability is being released at SST values that are too low. Again, this likely points to a shortcoming with the convective parameterization and/or with the boundary layer formulation.

5. Summary and Conclusions

The objective of this study was to assess the quality of the ocean surface heat flux fields simulated by the NOGAPS 3.4 forecast model run in climate simulation model (referred to here as NOGAPS-CL). Comparisons were made between a 17-year NOGAPS-CL simulation using observed SSTs as surface boundary conditions and a number of validating data sets consisting of ship, satellite, and/or reanalysis-based surface heat flux, precipitation, TOA radiation budget, water vapor, cloud frequency, and wind products. The heat flux comparisons focused primarily on the shortwave and latent heat fluxes over the tropical oceans, as this region is where the largest errors were typically found. The results indicate that the climate simulation using the NOGAPS-CL model underpredicts the net surface shortwave flux by about 30-50 W m-2 in much of the subtropical oceans (Figure 1) and overpredicts the net shortwave flux in the western Pacific warm pool and the midlatitude oceans by about 30-50 W m-2. Compounding this error is a bias in the latent heat flux with a somewhat similar spatial structure. In much of the subtropics, NOGAPS-CL overpredicts the latent heat flux by about 40-60 W m-2 and under predicts the latent heat flux over the northern ocean western boundary currents by about 30-50 W m-2 (Figure 2). While many of the areas of negative bias in shortwave flux and positive bias in latent heat fllux overlap in the subtropics, the maxima in evaporation bias actually tend to lie slightly "upwind" from the minima in shortwave flux bias. Even so, in many subtropical areas the biases in the shortwave and latent heat flux combine to produce considerable errors in the surface net heat flux, with too little heat entering the subtropical/tropical oceans (~ 50-70 W m-2) and too much heat loss in the midlatitudes (~50-70 W m-2, Figure 3).

To try and understand the basis for the shortwave and latent heat flux biases, particularly in the tropics, a number of other model-data comparisons were made. These included comparisons to observed values of precipitation (Figure 6), precipitable water (Figure 8), TOA longwave and shortwave fluxes for both clear-sky and all-sky conditions (Figures 4,5,7, and 9), as well as cloud frequency measures for total, low-, middle-, and high-level clouds (Figures 10-13). From these comparisons it was determined that the shortwave flux biases in the subtropical regions are the result of too many middle- and high-level clouds being produced by the climate model near the edges of the deep convective zones. This is related to the production of too much rainfall and too little outgoing longwave radiation in these same regions. The shortwave flux biases in the deep convective zones, such as the Indo-Pacific warm-pool, are the result of too few clouds, especially high level clouds. Collocated with this positive

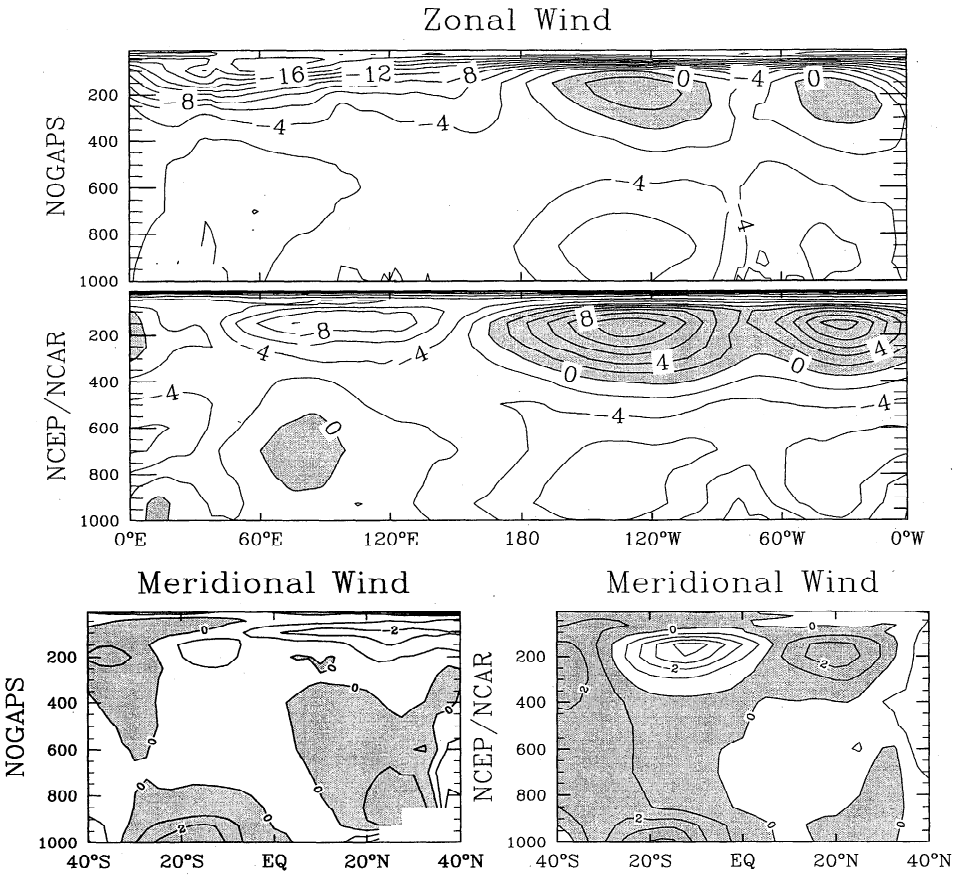

Figure 17. (top) Long-term mean zonal wind averaged between 15°N and 15°S from the NOGAPS-CL simulation (top) and the NCEP/NCAR reanalysis (bottom). (bottom) Long-term mean meridional wind averaged between 60°E and 120°E from the NOGAPS-CL simulation (left) and the NCEP/NCAR reanalysis (right). Contours are every 2 (1) m s^{-1} for zonal (meridional) wind.

shortwave bias is a significant dry bias in the tropospheric water vapor content. These cloud and water vapor biases (in addition to the large-scale circulation changes associated with them; see below) have the additional impacts of producing too little precipitation and too much outgoing longwave radiation in this region.

When the above biases are considered together, the results suggest that the moist static energy in the boundary layer is being prematurely released in the subtropical regions near the deep convective regions. This ends up impacting the climatological hydrological cycle and the large-scale circulation. First, since the deep convection triggers prematurely, there are too many clouds being formed outside the deep tropics and too much precipitation falling in these areas. The biases in precipitation induce biases in the surface wind convergence, with the winds normally upstream (downstream) of the convection being increased (decreased) in magnitude and leading to an increase (decrease) in surface evaporation (Figure 15). Moreover, since too much moist static energy is being released before it arrives in the warmest regions of the tropics (i.e., where precipitation is normally greater than evaporation due to the large-scale convergence), the amount of available moisture in these regions is diminished. This results in reduced cloudiness and rainfall and increased shortwave flux and outgoing longwave radiation in the climate simulation. The diminished rainfall (i.e. latent heating) and longwave radiation trapping reduces the strength of the large-scale circulation (Figures 16 and17), which in turn reduces the strength of the subsidence in the subtropical regions which is, in part, supposed to help suppress the convection processes in these regions which are prematurely triggering. Thus the feedbacks in this process are coupled and involve surface flux, convection, clouds, and the dynamics.

A schematic illustration of the feedbacks described above is given in Figure 14. Additional evidence for the above scenario is given in a distribution of rainfall versus SST for the tropical regions, which shows that the peak rainfall amounts are falling over SSTs of about 28oC, when the observed distribution indicates that peak rainfall values occur over 29.5oC (Figure 18). These results are consistent with the results of Ridout and Reynolds [1998]. They show that reducing excessive precipitation in the trade wind regime through the use of a boundary layer thermal convective-triggering mechanism allows for an increased flux of moisture into the warm-pool region. This in turn leads to an increase in the precipitation over the warm pool and improved precipitation, precipitable water, and low-level winds in that region. Note that considering the magnitudes of the biases highlighted in this study, it would not appear

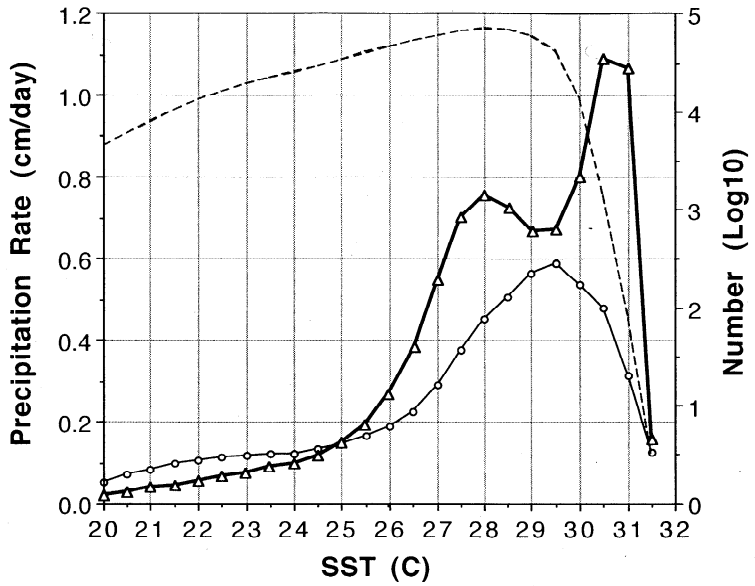

Figure 18. Distributions of precipitation rate versus sea surface temperature (SST) from the NOGAPS-CL simulation (thick) and the MSU observations (thin). The distributions are derived from the region 30°N to 30°S for the years 1979 to 1993. The dashed line indicates the number of values in each SST bin.

that the results nor their interpretation are likely to be too sensitive to the cited errors in the long-term mean values of the observations used in the model-data comparisons.

While the biases in the NOGAPS-CL simulation discussed above are associated with the mean climate, it is possible that these same physical shortcomings are affecting some transient systems in the climate simulation as well. For example, the NOGAPS-CL simulation exhibits very weak intraseasonal variability (not shown; see also Reynolds and Gelaro [1996]), a feature quite common among many of the AMIP participants [Slingo et al., 1996]. While there is some theoretical evidence [Wang and Xie, 1998] that ocean-atmospheric coupling is necessary to properly simulate the Madden-Julian Oscillation (MJO) [Madden and Julian, 1994], modeling studies suggest that ocean coupling acts to improve an already existing MJO [Waliser et al., 1999a; cf. Sperber et al., 1997]. Assuming that the phenomenon can be simulated with some success without coupling, then it is possible that the moist static energy is not allowed to build up over the large space and timescales required to foster a viable MJO. A recent modeling study by Wang and Schlesinger [1999] provides some support for this hypothesis. They showed that using either the Arakawa-Schubert, moist-convective adjustment, or Kuo convective parameterizations in the same GCM produces significant MJO variability only when the critical moisture for deep convection to occur is made sufficiently high (~ >90%). This suggests that any early triggering of convection that may be occurring in the NOGAPS-CL model is probably adversely impacting the development of the MJO (a transient that may or not be affecting the mean) as well as the mean climate itself.

The above comments regarding the MJO appear consistent with results obtained by Ridout and Reynolds [1998] from a single winter (1987/1988) integration of a T47L18 version of NOGAPS. In that study, the authors identified a deficiency of precipitation in the warm pool region of the western Pacific and too much precipitation in the trade wind region to the north. The present results help to establish the climatological and global significance of this problem. Although Ridout and Reynolds were able to largely correct the precipitation bias for the 1987/1988 winter integration by introducing a boundary layer regime-based convective-triggering scheme that reduces the occurrence of deep convection over the trade wind regime, the efficacy of this treatment over longer time periods and regions outside the tropical Pacific was not addressed. Their analysis also showed that the new convective trigger formulation yielded improvements in precipitable water and low-level winds in the tropical Pacific, but the response of other fields to the treatment, such as the bias in the surface latent heat flux identified in the present work, was not examined.

Finally, on the basis of the results from a number of AMIP-related studies, there appears to be significant commonality between the bias structures evident in NOGAPS-CL and the participating models in AMIP. Some of the shared features noted include the biases in precipitation [Lau et al., 1996], water vapor [Duvel et al., 1997], and evaporation [Gleckler and Weare, 1997], as well as the weak representation of the MJO [e.g., Slingo et al., 1996]. The consideration in this study of a more wide range of fields/processes (e.g., surface fluxes, water vapor, TOA radiation fluxes, large-scale flow) associated with a single model has led us to a more inclusive understanding of the root of the problem for a wide range of model-observation differences. To the extent that the overall model biases found in NOGAPS-CL are common among many GCMs, then the physical scenario and associated discussion concerning convective triggering and parameterization might also apply. Such a recognition, based on analysis of other models featuring similar biases, might help to focus model development efforts on processes that would likely have the greatest impact on improving our simulations of climate.

Acknowledgments. Support for this study was provided by the Atmospheric Modeling and Prediction Division of the Office of Naval Research under grant N000149710527 (DW) and Office of Naval

Research grant 0602435N (TH). We would like to thank Jim Ridout, Carolyn Reynolds, and Gregory Rohaly (NRL) for providing a number of useful discussions and comments. We would also like to thank Zhanqing Li for providing the Li et al. shortwave data set for this study and Ralph Ferraro for providing the SSM/I precipitable water. This study's analysis and presentation greatly benefited from the use of Seaspace Corporation's TeraScan software system and the NCAR Graphics Package. Computing support was provided by the Department of Defense High-Performance Computing Program.

References

Barkstrom, B. R., The Earth Radiation Budget Experiment (ERBE), Bull. Am. Meteorol. Soc., 65, 1170-1185, 1984.

Beljaars, A. C. M., The impact of some aspects of the boundary layer scheme in the ECMWF model, in Proceeding of the ECMWF Workshop on Parameterization of Sub-grid Scale Processes. Eur. Cent. for Medium-Range Forecasts, Reading, England, 1995.

Briegleb, B. P., Delta-Eddington approximation for solar radiation in the NCAR Community Climate Model, J. Geophys. Res., 97, 7603-7612, 1992.

da Silva, A., A. C. Young, and S. Levitus, Atlas of Surface Marine Data 1994, Volume 1, Algorithms and Procedures, NOAA Atlas NESDIS 6, U.S. Dep. of Comm., Washington, D. C., 1994.

Duvel, J. P., S. Bonyl, H. Le Treut, and Participating AMIP Modeling Groups, Clear-sky greenhouse effect sensitivity to sea surface temperature changes: An evaluation of AMIP-simulations, Clim. Dyn., 13, 259-273, 1997.

Ferraro, R., F. Weng, N. Grody and A. Basist, An eight year (1987-1994) time series of rainfall, clouds, water vapor, snow-cover, and sea-ice derived from SSM/I measurements. Bull. Am. Meteorol. Soc. 77, 891-905, 1996.

Fouquart, Y., B. Bonnel, and V. Ramaswamy, Intercomparing shortwave radiation codes for climate studies, J. Geophys. Res., 96, 8955-8968, 1991.

Gaffen, D., D. Rosen, D. Salstein, and J. Boyle, Evaluation of tropospheric water vapor simulations from the Atmospheric Model Intercomparison, J. Clim., 10, 1648-1661, 1997.

Gates, L. W., An overview of the results of the Atmospheric Model Intercomparison Project (AMIP), Bull. Am. Metor. Soc., 80, 29-56, 1999.

Gill, A. E., Some simple solutions for heat-induced tropical circulation, Q. J. R. Meteorol. Soc., 106, 447-462, 1980.

Gleckler, P. J., and B. Weare, Uncertainties in global ocean surface heat flux climatologies derived from ship observance, J. Clim. 10, 2763-2781, 1997.

Hack, J. J., B. A. Boville, B. P. Briegleb, J. T. Kiehl, P. J. Rasch, and D. L. Williamson, Description of the NCAR Community Climate Model (CCM2), NCAR/TN-382+STR, 108 pp, Natl. Cent. For Atmos. Res., Boulder, Colo.,1993.

Harshvardhan, R. Davies, D. Randall, and T. Corsetti, A fast radiation parameterization for atmospheric circulation models, J. Geophys. Res., 92, 1009-1016, 1987.

Hartmann, D. L., V. Ramanathan, A. Berroir, and G. E. Hunt, Earth radiation budget data and climate research, Rev. Geophys., 24, 439-468, 1986.

Hogan, T., and L. Brody, Sensitivity studies of the Navy's global forecast model parameterizations and evaluation of improvements to NOGAPS, Mon. Weather Rev., 121, 2373-2395, 1993.

Hogan, T. F., and T. E. Rosmond, The description of the Navy Operational Global Atmospheric Prediction System's spectral forecast model, Mon. Weather Rev., 119, 1786-1815, 1991.

Jing, X., and R. D. Cess, Comparison of atmospheric clear-sky radiation models to collocated satellite surface measurements in Canada, J. Geophys. Res., 103, 28,817-28,824, 1998.

Josey, S. A., E. C. Kent, and P. K. Taylor 1999: New insights into the ocean heat budget closure problem from analysis of the SOC air-sea flux climatology, J. Clim., 12, 2856-2880 1999.

Kalnay, E., et al., NCEP/NCAR 40-Year Reanalysis Project, Bull. Am. Meteor. Soc., 77, 437-471, 1996.

Kiehl, J. T., J. J. Hack, G. B. Bonan, B. A. Boville, D. L. Williamson, and P. J. Rasch, The National Center for Atmospheric Research Community Climate Model: CCM3, J. Clim., 11, 1131-1150, 1998.

Lau, K.-M, J. H. Kim, and Y. Sud, Intercomparison of hydrologic processes in AMIP GCMs, Bull. Am. Metor. Soc., 77, 2209-2227, 1996.

Li, T., and T. Hogan, The role of the annual-mean climate on season and interannual variability of the tropical Pacific in a coupled GCM, J. Clim., 12, 780, 1999.

Li, Z., H. G. Leighton, K. Masuda, and T. Takashima, Estimation of SW flux absorbed at the surface from TOA reflected flux, J. Clim., 6, 317-330, 1993a.

Li, Z., H. G. Leighton, and R. D. Cess, Surface net solar radiation estimated from satellite measurements: Comparisons with tower observations, J. Clim., 6, 1764-1772, 1993b.

Li, Z., C. H. Whitlock, and T. P. Charlock, Assessment of global monthly mean surface insolation estimated from satellite measurements using Global Energy Balance Archive data, J. Clim., 8, 315-328, 1995.

Louis, J. F., A parametric model of vertical eddy fluxes in the atmosphere, Boundary Layer Meteorol., 17, 187-202, 1979.

Louis, J. F., M. Tiedtke, and J. F. Geleyn, A short history of the operational PBL parameterization at ECMWF, in ECMWF Workshop on Planetary Boundary Parameterizations, pp. 59-79, 1Eur. Cent. for Medium-Range Forecasts, Reading, England, 982.

Ma, C.-C., C.R. Mechoso, A. Arakawa, and J.D. Farrara, Sensitivity of a coupled ocean-atmosphere model to physical parameterizations, J. Clim., 7, 1883-1896, 1994.

Madden, R. A., and P. R. Julian, Observations of the 40-50 day tropical oscillation: A review, Mon. Weather Rev., 112, 814-837, 1994.

Meehl, G. A., Modification of surface fluxes from component models in global coupled models, J. Clim., 10, 2811-2825, 1997.

Moorthi, S., and M. Suarez, Relaxed Arakawa-Schubert: A parameterization of moist convection for general circulation models, Mon. Weather Rev., 120, 978-1002, 1992.

Nelson, C., and W. Aldinger, An overview of Fleet Numerical Oceanography Center operations and products, Weather Forecasting, 7, 204-219, 1992.

Oberhuber, J. M, An atlas based on the COADS data set. Tech. Rep. 15, Max-Planck-Inst. Fur Meteorol., Hamburg, Germany, 1988.

Ohmura, A., and H. Gilgen, Global Energy Balance Archive (GEBA). World Climate Program – Water Project A7, Report 2: The GEBA Database, Interactive Application, Retrieving Data, 60 pp, Verlag der Fachvereine, 1991.

Palmer, T. N., G. J. Shutts, and R. Swinback, Alleviation of a systematic westerly bias in general circulation and numerical weather prediction models through an orographic gravity wave drag parameterization, Q. J. R. Meteorol. Soc., 112, 1001-1039, 1986.

Pinker, R., and I. Laszlo, Modeling surface solar irradiance for satellite applications on a global scale, J. Appl. Meteorol., 31, 194-211, 1992.

Reynolds, C., and R. Gelaro, The effect of model bias on the equatorial propagation of extratropical waves, Mon. Weather Rev., 125, 3249-3265, 1997.

Reynolds, C., R. Gelaro, and T. Murphee, Observed and simulated Northern Hemisphere intraseasonal circulation anomalies and the influence of model bias, Mon. Weather Rev., 124, 1100-1118, 1996.

Ridout, J. A., and C. Reynolds, Western Pacific warm pool region sensitivity to convective triggering by boundary layer thermals in the NOGAPS AGCM, J. Clim., 11, 1553-1573, 1998.

Rosmond, T. E., A prototype fully coupled ocean-atmosphere prediction system, Oceanography, 5, 25-30, 1992.

Rossow, W.B., and R. A. Schiffer, ISCCP cloud data products, Bull. Am. Meteor. Soc., 72, 2-20, 1992.

Slingo, J.M., The development and verification of a cloud prediction for the ECMWF model, Q. J. R. Meteorol. Soc., 113, 899-927, 1987.

Slingo, J. M., et al., Intraseasonal oscillations in 15 atmospheric general circulation models: Results from an AMIP diagnostic subproject, Clim. Dyn., 12, 325-357, 1996.

Spencer, R. W., Global oceanic precipitation from the MSU during 1979-91 and comparisons to other climatologies, J. Clim., 6, 1301-1326, 1993.

Sperber, K. R., J. M. Slingo, P. M. Inness, and K. M. Lau, On the maintenance and initiation of the intraseasonal oscillation in the NCEP/NCAR reanalysis and the GLA and UKMO AMIP simulations, Clim. Dyn. 13, 769-795, 1997.

Tiedtke, M., The sensitivity of the time-mean flow to cumulus convection in the ECMWF model, in ECMWF Workshop on Convection in Large-Scale Numerical Models, pp. 297-316, Eur. Cent. for Medium-Range Forecasts, Reading, England, 1984.

Waliser, D. E., and N. E. Graham, Convective cloud systems and warm-pool SSTs: Coupled interactions and self-regulation. J. Geophys. Res. 98, 12881-12893, 1993.

Waliser, D. E., W. K. Lau, and J. H. Kim, The influence of coupled sea

surface temperatures on the Madden Julian Oscillation: A model perturbation experiment, J. Atmos. Sci., 56, 333-358, 1999a.

Waliser, D. E., Z. Shi, J. Lanzante, and A. Oort, The Hadley circulation: Assessing reanalysis and sparse in-situ estimates, Clim. Dyn., 15, 719-735 1999b.

Waliser, D. E., R. A. Weller, R. D. Cess, Comparisons between buoy-observed, satellite-derived and modeled surface shortwave flux over the subtropical North Atlantic during the Subduction Experiment, J. Geophys. Res., in press, 1999c.

Wang, W., and M. E. Schlesinger, The dependence on convective parameterization of the tropical intraseasonal oscillation simulated by the UIUC 11-layer atmospheric GCM, J. Clim., 12, 1423, 1999.

Wang, B., and X. Xie, Coupled modes of the warm pool climate system, part I, The role of air-sea interaction in maintaining Madden Julian Oscillation, J. Clim., 11, 2116-2135, 1998.

Weare, B. C., Uncertainties in estimates of surface heat fluxes derived from marine reports over the tropical and subtropical oceans, Tellus, Ser. A, 41, 357-370, 1989.

Weare, B. C., and I. Mokhov, Evaluation of total cloudiness and its variability in the Atmospheric Model Intercomparison Project, J. Clim., 8, 2224-2238, 1995.

Whitlock, C. H., et al., First global WCRP shortwave surface radiation budget dataset, Bull. Am. Meteorol. Soc., 76, 905-922, 1995.

Wielicki, B. A., R. D. Cess, M. D. King, D. A. Randall, and E. F. Harrison, Mission to planet earth: Role of clouds and radiation in climate, Bull. Am. Meteorol. Soc., 76, 2125-2153, 1995.

Xie, P., and P. A. Arkin, Global precipitation: A 17-year monthly analysis based on gauge observations, satellite estimates, and numerical model outputs, Bull. Am. Meteorol. Soc., 78, 2539-2558, 1997.

Zhang, M. H., Implication of the convection-evaporation-wind feedback to surface climate simulation in climate models, Clim. Dyn., 12, 299-312, 1996.

Zender, C. S., S. Pope, B. Bush, A. Bucholtz, W. D. Collins, J. T. Kiehl, F. P. J. Valero, and J. Vitko, Atmospheric absorption during ARESE, J. Geophys. Res., 102, 29,901-29,915, 1997.

D. E. Waliser, Institute for Terrestrial and Planetary Atmospheres, Endeavour Hall 205, State University of New York, Stony Brook, NY, 11794-5000. (waliser@terra.msrc.sunysb.edu)

T. F. Hogan, Naval Research Laboratory, 7 Grace Hopper Ave., Monterey, CA 93943-5502. (hogan@nrlmry.navy.mil)

(Received December 16, 1998; revised September 14, 1999; accepted September 22, 1999.)